Journal of Catalysis 388 (2020) 38–51

Contents lists available at ScienceDirect

Journal of Catalysis

journal homepage: www.elsevier.com/locate/jcat

Ab initio enhanced sampling kinetic study on MTO ethene methylation reaction

Simon Bailleul [1], Karen Dedecker [1], Pieter Cnudde, Louis Vanduyfhuys, Michel Waroquier, Veronique Van Speybroeck *

Center for Molecular Modeling (CMM), Ghent University, Technologiepark 46, B-9052 Zwijnaarde, Belgium

ARTICLE INFO

Article history:
Received 10 October 2019
Revised 31 March 2020
Accepted 16 April 2020
Available online 25 April 2020

Keywords:
Collective variables
DFT
Enhanced sampling
Molecular dynamics
Ethene methylation
ZSM-5

ABSTRACT

The methylation reaction of ethene with methanol over the Brønsted acidic ZSM-5 catalyst is one of the prototype reactions within zeolite catalysis for which experimental kinetic data is available. It is one of the premier reactions within the methanol-to-olefins process and has been the subject of extensive theoretical testing to predict the reaction rates. Herein, we apply, for the first time, first principle molecular dynamics methods to determine the intrinsic reaction kinetics taking into account the full configurational entropy. As chemical reactions are rare events, enhanced sampling methods are necessary to obtain sufficient sampling of the configurational space at the activated region. A plethora of methods is available which depend on specific choices like the selection of collective variables along which the dynamics is enhanced. Herein, a thorough first principle molecular dynamics study is presented to determine the reaction kinetics via various enhanced MD techniques on an exemplary reaction within zeolite catalysis for which reference theoretical and experimental data are available.

© 2020 Elsevier Inc. All rights reserved.

1. Introduction

In the last decades, significant progress has been made in the field of computational zeolite catalysis [1]. New methods entered the scene such as advanced molecular dynamics methods – we refer to Refs. [2,3] for some recent reviews – , which have the potential to model chemical reactions at operating conditions [1,4–6]. These techniques can help us to optimize the design of heterogeneous catalysts, for which a thorough understanding of elementary reaction steps on a molecular level is crucial. Solely based on experimental data, it has been shown to be extremely challenging to gather such information due to the large number of reactions that take place simultaneously. However, this hurdle can be overcome by complementing the experimental information with theoretical simulations [7–15]. It is generally accepted that ab initio predictions attain chemical accuracy if they reproduce energy barriers within an error bar less than 1 kcal/mol (4.2 kJ/mol) and that they attain kinetic accuracy when the factor $f_k = k_{theory}/k_{experiment}$ (with k_i the reaction rate constant) deviates less than one order of magnitude [4,16–19].

A seminal contribution in this field was done by Piccini et al. [20] who proposed a divide-and-conquer strategy, which enabled to attain chemical accuracy for the methylation of ethene, propene and *trans*-2-butene over the zeolite catalyst H-ZSM-5. These methylation reactions, depicted schematically for ethene in Scheme 1, are of utmost importance in the methanol-to-olefins (MTO) process and are therefore frequently used as a dataset for the benchmarking of theoretical procedures [17,19,20]. It is one of the few reactions within zeolite catalysis for which kinetic experimental data are available by meticulously tuning the experimental conditions [21,22]. The MTO process is of industrial relevance as it is one of the most prominent technologies to bypass crude oil in the production of light olefins, like ethene and propene [23–25]. The governing reaction mechanism has been a point of discussion in the last decade, but intensive research led to a general consensus on the hydrocarbon pool (HP) mechanism in which organic compounds, present in the zeolite pores, act as a co-catalyst in the conversion of methanol to olefins [26–30]. Two interacting reaction cycles have been proposed, namely the alkene and aromatic cycle, which differ by the type of HP species considered [23,24,31,32]. Earlier studies showed that methylation reactions of the co-catalysts are elementary reaction steps, as they are responsible for the growth of the HP species [5,21,22,33–37].

One of the main conclusions of the work of Piccini et al. [20] is the importance of accounting for anharmonic corrections in the

* Corresponding author.
E-mail address: veronique.vanspeybroeck@ugent.be (V. Van Speybroeck).
[1] Authors contributed equally.

https://doi.org/10.1016/j.jcat.2020.04.015
0021-9517/© 2020 Elsevier Inc. All rights reserved.

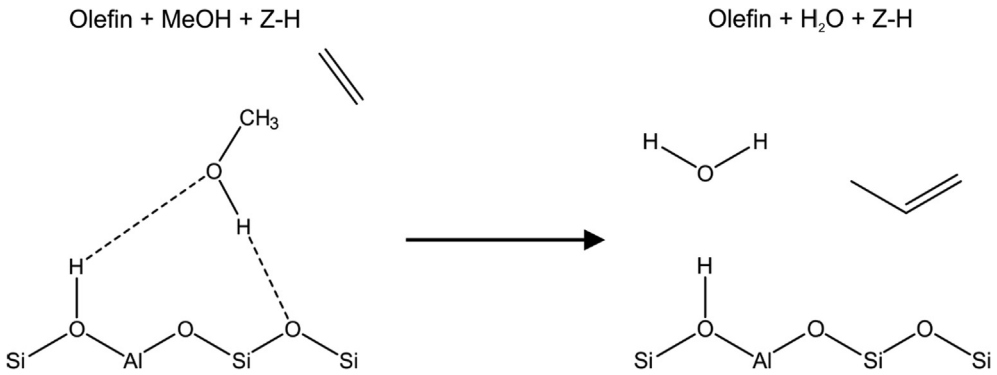

Scheme 1. Schematic representation of the methylation of ethene with methanol yielding propene.

calculation of enthalpy barriers and rate constants. In principle, molecular dynamics (MD) based techniques allow accounting for anharmonic effects in a rather natural way, however the disentanglement of entropic an enthalpic contributions remains problematic [4,38–40]. In contrast to static calculations which are limited to a few stationary points at 0 K (namely reactant, transition state and product), MD techniques have the advantage that a larger portion of the potential energy surface (PES) is sampled [4,5]. For methylation reactions in large pore zeolites like AFI, it was shown that not one single transition state could be found but various quasi-isoenergetic complexes were localized. In this case, it is more appropriate to introduce the concept of an activated region [7]. Besides the computational effort, the main disadvantage of regular MD is that sampling is limited to the most probable states of the system, making the sampling of states high in energy, like transition states, rare events [41,42]. Sampling of these improbable regions can be achieved by applying advanced molecular dynamics or enhanced sampling techniques [41,42]. Three components have to be taken into account when performing free energy calculations, namely: [3,42,43]

(i) The choice of a suitable model for the Hamiltonian
(ii) The selection of the sampling protocol to explore all relevant parts of the PES
(iii) The choice of the estimator to obtain the free energy difference [44]

First of all, for the selection of the Hamiltonian, one needs to compromise between the accuracy and efficiency of the model [42]. In this case where chemical bonds are constantly broken and formed it is mandatory to use a quantum mechanical description of the system rather than a force field based approach. Albeit force fields are computationally much more efficient, one would have to turn to reactive force fields such as ReaxFF, however there are still some limitations to this approach [45,46]. Currently, DFT based methods are commonly used as a compromise between accuracy and efficiency compared to more expensive (post-)HF wave function based methods such as RPA [47,48]. In this work, a pragmatic approach is followed by using DFT calculations with Grimme (D3) dispersion interactions [49], as employed in previous studies [1,4,17,19]. Some caution needs to be taken into account in interpreting the absolute quantitative values as the energies might be sensitive to the dispersion correction scheme and choice of the exchange–correlation functional [4,17,19,20,50]. However, this is not the topic of the current study.

Secondly, a sampling protocol to visit the relevant parts of the PES must be selected. This protocol can be based on Molecular Dynamics and/or Monte Carlo simulations [42,43] but in this work, MD based methods are chosen. As the reported reaction barriers are significantly higher [17,19–22], enhanced sampling methods are necessary. A plethora of enhanced sampling methods has been proposed in literature [2,3,41,42].

In principle the multidimensional free energy surface (FES) can be investigated with any sampling protocol by defining an appropriate set of collective variables which are a function of the microscopic coordinates of the system. Herein, we employ the definition of a collective variable (CV) introduced in the work of Peters [51] and applied in a seminal paper of Demuynck et al. [52] in the framework of phase transformations in Metal Organic Frameworks (MOFs).

A proper collective variable should satisfy three requirements: [51]

(i) The CV should only depend on the instantaneous point in configuration space
(ii) The CV should vary monotonically while moving from the reactant over the transition state to the product
(iii) Projection of the free energy on the CV should result in a one-dimensional free energy profile with reduced dynamics which are consistent with the full phase space.

The selection of a collective variable is of utmost importance, though not always straightforward (vide infra) [43,51–53]. If these variables are hard to identify, all degrees of freedom can be enhanced, for example by increasing the temperature as applied in replica exchange [54–56]. On the other hand, if these functions are known, enhancement of the sampling can be limited to CVs only [2,41,42,52]. Examples of enhanced sampling techniques include umbrella sampling (US) [57–59], thermodynamic integration (TI) [60–66], metadynamics (MTD) [67–69] and variationally enhanced sampling (VES) [70–72].

As prescribed by step (iii), the estimator to obtain the free energy from the sampling needs to be chosen. Most sampling methods are correlated with a particular estimator [44]. Umbrella sampling uses several bias potentials from which the free energy surface (FES) is estimated with for instance the weighted histogram method (WHAM) [73,74]. In the Blue Moon method, the FES can be reconstructed from the constrained simulations using thermodynamic integration [60]. Furthermore, as metadynamics is based on adapting the bias potential by adding Gaussian hills, and variationally enhanced sampling on adapting the bias potential based on the variational principle, the inverted final bias can be used as an estimate of the FES [68,69,71].

In this work, several enhanced sampling methods will be tested and benchmarked for the methylation of ethene in H-ZSM-5 as a case study [17,19–22]. Since several collective variables can be selected to simulate this reaction, as proposed in Section 2.4, different CVs will be tested using umbrella sampling. To allow a

proper comparison, the free energy profiles need to be transformed from one CV to another. This will allow us to study in how far the kinetic data depend on the particular choice of CV. Subsequently, the obtained barriers are validated by comparison with available static DFT calculations and experimental data. To compare with existing literature data, [17,19–22] the relation needs to be made between intrinsic and apparent reaction rates. Since our MD results yield intrinsic kinetics, additional static calculations [11,48,75–77] are performed to overcome this hurdle, as discussed in the last part of this work. The current study presents a fundamental methodological benchmark for various enhanced MD techniques on an exemplary reaction within zeolite catalysis.

2. Computational details and theoretical background

2.1. Catalyst model

The H-ZSM-5 catalyst exhibits the MFI topology, characterized by a 3D network of sinusoidal and straight 10-ring channels leading to medium sized pores [78]. All simulations are performed using a periodically extended unit cell of H-ZSM-5 consisting of 96 T atoms. In this unit cell, one silicon atom is replaced by an aluminum atom to create the Brønsted acid site (BAS). There is no simple rule for the occupation of Al atoms on the 24 distinguishable framework T sites, because it depends on the conditions of the zeolite synthesis [79]. Analogous to earlier work, the substitution is performed at the T12 position, at the intersection of the straight and sinusoidal channels [80,81]. The unit cell volume used in the static calculations is optimized at 0 K, while the unit cell parameters for the dynamic simulations are equilibrated at 623 K. The equilibration procedure and resulting unit cell parameters are described in Section 1 and Table S1 of the ESI.

2.2. Reference static calculations

Apart from the MD based simulations, also reference static Density Functional Theory calculations are performed [11,75–77] with the Vienna Ab Initio Simulations Package (VASP 5.3) [82–85]. The revPBE functional [86] is chosen because of its improved performance for solid-state calculations compared to the commonly used PBE functional [87]. Additionally, Grimme D3 dispersion corrections are added to account for attractive London dispersion interactions [49]. Other specifications are the use of the projector augmented wave (PAW) method and a plane-wave cutoff of 600 eV. We imposed an electronic energy convergence criterion of 10^{-5} eV together with an ionic relaxation threshold of 10^{-4} eV [88,89]. During the VASP calculations, the Brillouin zone sampling is restricted to the Γ-point. Transition states are initially optimized with the improved dimer method of Heyden et al. [90] and then refined with a quasi-Newton algorithm as implemented in VASP [91]. Geometries are slightly displaced along the normal mode corresponding to the motion that leads the system over the barrier to generate starting geometries for the optimization of reactant and product states. For these calculations, a conjugate gradient algorithm is applied [92].

Since partial Hessian vibrational analysis (PHVA) is shown to be an attractive alternative for computationally demanding full Hessian vibrational analysis (FHVA) for entropy calculations, this scheme is used for the normal mode analysis (NMA) in this work using TAMkin [93,94]. In a PHVA calculation, only a part of the system is taken into account during the NMA, namely the guest molecules and the 8 T cluster of the framework around the active site indicated in Figure S1 of the ESI.

2.3. Molecular dynamics

To equilibrate the volume and unit cell parameters at operating conditions, i.e. 623 K and 1 atm, regular ab initio molecular dynamics simulations in the NPT ensemble are performed using the CP2K software package [95,96]. During the ab initio MD simulations, the temperature is controlled by a chain of five Nosé-Hoover thermostats [38] and the pressure by an MTK barostat [97]. Again, the revPBE functional [86] is chosen because of its improved performance for solid-state calculations compared to the commonly used PBE functional [87]. Furthermore, the combined Gaussian and Plane Wave (GPW) basis sets approach is used [98,99]. The DZVP-GTH basis set and pseudopotentials [100] were used, and Grimme D3 dispersion corrections [49] are added. The time step for integration of the equations of motion is set to 0.5 fs. All systems are first equilibrated for 5 ps, followed by a production run of 50 ps in the NPT ensemble to obtain the average unit cell parameters and volume. All subsequent regular and enhanced sampling MD simulations are carried out in the NVT ensemble, as explained in Section 1.2 of the ESI, keeping the unit cell parameters and thus the volume constant.

Further details on the enhanced sampling MD simulations are given in Section 2.5.

2.4. Collective variables

2.4.1. Possible collective variables

Several collective variables can be proposed which may act as suitable reaction coordinates to enhance sampling along the ethene methylation reaction path in HZSM-5. Herein, two types of CVs are applied, visually displayed in Fig. 1. One type (type CN) consists of coordination numbers (CNs) between two atoms describing the breaking and formation of the C-O and the C-C bond [4,101,102]. CN_{ij} represents the coordination number between the atoms i and j defined as:

$$CN_{ij} = \sum_{i,j} \frac{1 - \left(\frac{r_{ij}}{r_0}\right)^{nn}}{1 - \left(\frac{r_{ij}}{r_0}\right)^{nd}}$$

with r_{ij} the interatomic distance and r_0 the reference distance, set to 2 Å, which approximately represents the C-C distance in the transition state. Furthermore, the parameters *nn* and *nd* where chosen to be 6 and 12, respectively. As such, two collective variables are needed to describe the methylation reaction: CV1 being the coordination number CN_{OC} between the oxygen and carbon of the methanol (green and red in Fig. 1) and CV2 being the coordination number CN_{CC} between the carbon of methanol and the two carbons of ethene (red and blue in Fig. 1).

The second type (type DI) of collective variables is based on the distances of the breaking and forming bonds. The first collective variable CV1 is simply the bond distance d between carbon and oxygen of the methanol. The second collective variable CV2 is the distance d_{CM} between the carbon of methanol and the center-of-mass of the ethene molecule.

Finally, we also introduce a one-dimensional collective variable (type 1D-DI), namely the difference d_{CM}-d between the two collective variables in variant DI. The option to choose a 1D-CV has the advantage that it seriously speeds up the sampling [68]. This 1D-CV is used in the first part of this work to compare the different enhanced sampling methods.

2.4.2. Transformations between various collective variables

When using different collective variables, one cannot straightforwardly compare free energies obtained in various CVs, as explained hereafter. Suppose one defines two sets of collective

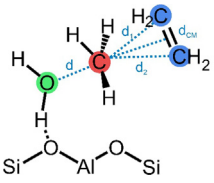

			CV1	CV2
Coordination numbers	Type CN		CN_{CC}	CN_{CC}
Distances	Type DI	DI	d	d_{CM}
		1D-DI	d_{CM}-d	-

Fig. 1. Schematic representation of the collective variables used to describe the methylation reaction of ethene. Their expected values at the reactant, transition and product state are summarized in Table S 2.

variables, q_1 and q_2, which have both the goal of describing the same process or reaction. If one would perform enhanced simulations using both collective variables, it would give rise to two free energy profiles, $F_{q_1}(q_1)$ and $F_{q_2}(q_2)$, which can in general not directly be compared since different collective variables give rise to different integrations over microstates. However, if both collective variables indeed describe the same process, the free energy profiles should be correlated. By means of statistical mechanics, as shown in Section 7 of the ESI, one can show that a free energy profile in terms of one collective variable can be transformed to a free energy profile in terms of another collective variable as:$F_{q_2}(q_2) = -k_B T \ln\left(\int_{-\infty}^{+\infty} p_{2|1}(q_2|q_1) e^{-\beta F_{q_1}(q_1)}\, dq_1\right)$

The derivation of the corresponding relation for 1D profiles is given in Section 7 of the ESI and in the work of Demuynck et al. [52].

Here, $p_{2|1}(q_2|q_1)$ is the conditional probability of the collective variable q_2 in terms of the collective variable q_1. The precision of this transformed free energy profile largely depends on the quality of the sampling of the phase space spanned by the variables q_1 and q_2. A sufficient sampling of coordinate q_2 for each relevant value of q_1 yields a proper conditional probability. In the frame of this work, it is useful to observe that the conditional probability can also be computed for simulations in which a bias along q_1 was applied (Section 7.2 of the ESI). The transformation is further illustrated in Fig. 2 for the case of 1D profiles, in which the integral is represented as an average of the Boltzmann probability weighted by the conditional probability (indicated by the shaded area on the figure).

Note that, in practice, we can apply this transformation from any reaction coordinate q_1 to another. The resulting free energy profile $F_{q_2}(q_2)$will only be realistic if the collective variable q_2 represents itself an appropriate reaction coordinate. Then the transformation from $F_{q_1}(q_1)$ to $F_{q_2}(q_2)$ should give the same result as a direct sampling simulation along q_2 and vice versa. This will be demonstrated in Section 3.2 of the Results and Discussion.

Finally, a one-dimensional projection of the obtained 2D free energy profile $F_{12}(q_1, q_2)$ is performed, as a 1D-profile is more convenient to interpret. This can be done by fixing a new collective variable q as a function of q_1 and q_2 ($q = q(q_1, q_2)$), and to perform an integration of the 2D probability distribution (also described in Section 7.3 of the ESI). An alternative is the elaborated search for the lowest free energy path [103]. In this work, the 2D profile is projected on the difference between the two collective variables ($q = q_2 - q_1$) as:

$$F_q(q) = -k_B T \ln\left(\int_{-\infty}^{+\infty}\int_{-\infty}^{+\infty} e^{-\beta F_{12}(q_1,q_2)} \delta(q - q_2 + q_1)\, dq_1\, dq_2\right)$$
$$= -k_B T \ln\left(\int_{-\infty}^{+\infty} e^{-\beta F_{12}(q_1, q_1+q)}\, dq_1\right)$$

2.5. Enhanced sampling methods

The enhanced sampling simulations are performed using the CP2K software package [95,96] interfaced with the advanced

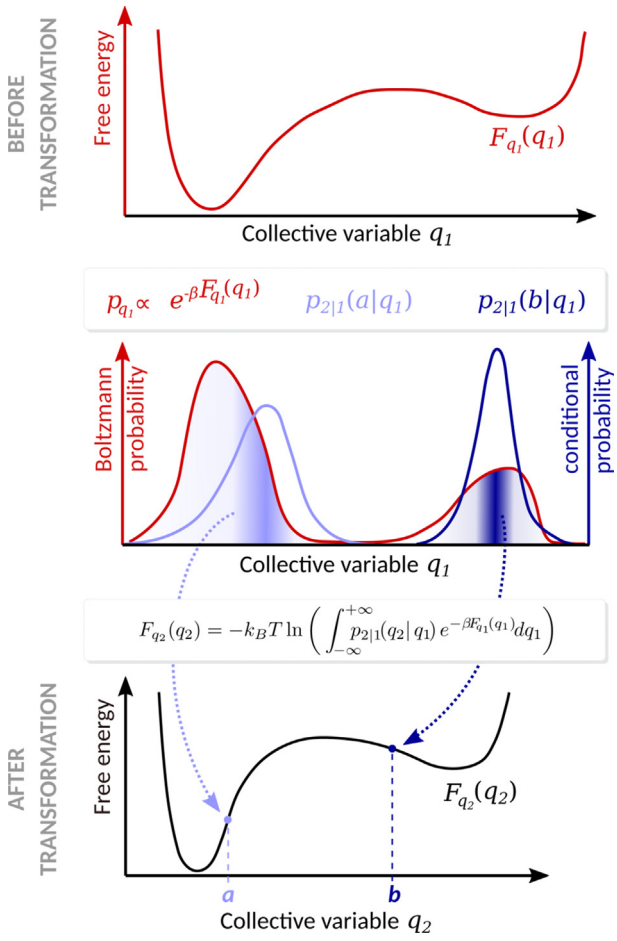

Fig. 2. Graphical representation of a free energy profile $\boldsymbol{F_{q_1}(q_1)}$, which was computed by sampling along $\boldsymbol{q_1}$ and expressed as a function of $\boldsymbol{q_1}$, and its transformation to the corresponding free energy profile $\boldsymbol{F_{q_2}(q_2)}$ as a function of $\boldsymbol{q_2}$. The integral can be interpreted as a weighted average of the Boltzmann probability, with weights given by the conditional probability and indicated through the shading in the middle pane.

simulations library PLUMED [104]. In this work, a selection is made of the variety of enhanced sampling techniques available in literature [2,3,41,42]: Metadynamics (MTD) [67,69], Variationally Enhanced Sampling (VES), Umbrella Sampling (US) and Thermodynamic Integration or Umbrella Integration (TI). The four methods are summarized in Figure S4 of the ESI, and a short summary of each methodology is given in Section S3 of the ESI. All chosen methods are able to enhance the sampling along certain degrees of freedom, the so-called collective variables. All selected methods rely on the introduction of a bias potential – which can vary depending on the method - allowing a decent sampling of all important and relevant regions of the configuration space.

(i) The **metadynamics (MTD)** technique is applied in this work to directly construct a one-dimensional free energy surface, by selecting a 1D reaction coordinate (1D-DI in Fig. 1). The bias potential is created on the fly by gradually adding Gaussian hills during the simulation. The width of the Gaussian potentials is set to 0.04 Å while the initial height is set to 5 kJ/mol and after each recrossing of the transition point, the height of the added hills is adequately halved to enhance the FES convergence, until a value of 0.3125 kJ/mol was obtained. A new hill was spawned every 100 time steps.

The integration time step is set to 0.5 fs for all MTD simulations. Furthermore, quadratic walls were used to restrict the

simulations to an area of interest on the FES, by limiting the diffusion of ethene and the formed water. Therefore, a quadratic upper wall is added at a value of 3.0 Å and a quadratic lower wall at −0.25 Å both with a force constant equal to 2000 kJ/(mol*Å^2). A total of 10 MTD simulations were performed, each with a sampling time between 250 and 300 ps.

(ii) **Variationally enhanced sampling (VES)** is a relatively new enhanced sampling technique introduced by Valsson and Parrinello [71] and recently applied in the construction of free energy profiles in structural transformations taking place in flexible MOFs [43]. The variational principle embedded in VES allows to introduce an arbitrary target distribution $p(q)$ that specifically targets the region of interest. In this work, a uniform target distribution was chosen. Furthermore, Legendre polynomials of the 25th order are taken as basis set. For the optimization algorithm, two parameters need to be chosen, namely the stride and step size. The stride is set to 100 time steps while the stepsize is first set to 5.0 kJ/mol and after some recrossings lowered to 1.0 kJ/mol, to have a similar procedure as in the metadynamics simulations. The same walls as in the metadynamics simulations are introduced to limit the sampling to the region of interest. A total of 5 VES simulations were performed, each with a sampling time between 300 and 350 ps.

(iii) In **umbrella sampling (US)** the reaction path is divided into 34–40 distinct windows, as summarized in Table S3 and Figure S4 of the ESI. In each window, a restrained ab initio MD simulation of 50–60 ps is run to ensure sufficient sampling and overlap between the different umbrellas. Initial configurations for each window are obtained from a moving restraint MD simulation in which a bias potential is displaced from the reactant to product minimum. The reaction coordinate is restrained to a target value q_i by applying a harmonic bias potential with a force constant, K, of 1500 kJ/mol for the coordination number or 1500 kJ/(mol*Å^2) for the distance CVs. Afterwards, the probability distributions of all windows are combined to a global distribution function using the weighted histogram analysis (WHAM) method [74,105].

(iv) In **thermodynamic integration (TI)** (or **Umbrella integration** following Kästner and Thiel [106]) the free energy difference between two configurations belonging to reaction coordinates q_0 and q_1 is then given by

$$\Delta F(q_0, q_1) = \int_{q_0}^{q_1} \langle \frac{\delta F}{\delta q} \rangle_q \, dq$$

in which $-\frac{\delta F}{\delta q}$ is the force needed to maintain the reaction coordinate constraint during the simulation. The constraint is imposed during the MD by introducing strong quadratic potentials. In this work we keep the 34–40 windows along the reaction coordinate which have been introduced during the umbrella sampling simulations of type 1D-DI, but the force constant K is set an order of magnitude higher. Again, for each window, a 50–60 ps restrained MD simulation is performed over which the mean force is calculated.

3. Results and discussion

In order to select the most appropriate sampling method, we make an assessment of the performance of the various enhanced sampling techniques proposed in the previous section [3,41–43]. Subsequently, the performance of different types of collective variables to describe the methylation of ethene, is tested using umbrella sampling as the most favorable enhanced sampling method for this specific reaction.

3.1. The influence of the enhanced sampling method on the intrinsic barrier

Four enhanced sampling methods are considered here, namely metadynamics (MTD), variationally enhanced sampling (VES), umbrella sampling (US) and thermodynamic integration (TI). For the selection of the most appropriate method, the sampling is performed using the one-dimensional collective variable, denoted type 1D-DI in Fig. 1. The main advantage of sampling in a one-dimensional space is the reduced computational cost [63,107]. As the efficiency of methods like metadynamics scale exponentially with the number of collective variables, a one-dimensional CV will speed up these simulations substantially [68]. The resulting free energy profiles are depicted in Fig. 3, together with an estimate of the corresponding error bars. The procedures for error estimation of all techniques are discussed in Section 5 of the ESI.

Several interesting conclusions can be drawn from Fig. 3. First, the four enhanced sampling methods give rise to a very similar free energy profile in the reactants side (up to the transition state TS) and similar forward energy barriers ranging between 102 and 107 kJ/mol. Furthermore, the small error bars for all simulations suggest decently converged results. This confirms the presumption that all enhanced sampling methods should give the same outcome, provided that we select good reaction coordinates and that the simulations are well converged.

The MTD and VES protocols require several barrier recrossings to obtain converged free energy estimates. For this specific reason, two walls are placed at well-chosen values of the one-dimensional collective variable (d_{CM}-d), as indicated in Fig. 3, to oppose the diffusion of ethene on the one hand, and to avoid sampling of the product state on the other hand. The reason is the instability of the primary product, protonated propene, as discussed in Section 6 of the ESI. Several products can be formed, e.g. propene, cyclopropane, propoxide, propanol,... This instability gives rise to the discrepancies observed for the US and TI results – which do not require restricting walls – in the product regime. The lower force constants used in US allow to converge to a more stable product, while the TI runs are stuck in a less stable product. As we are only interested in the forward barrier, the difference in sampling of the product region does not give rise to a preference for one specific technique.

A determining factor in the selection of the most suited enhanced sampling method will be the sampling efficiency. Considering the simulation times for all four methods (250–300 ps for MTD, 300–350 ps for VES, 50–60 ps per window – for a total of 40 windows – for US and TI), we prefer US and TI over the former two techniques. Whereas the total simulation time for the construction of a converged US or TI free energy profile will amount to over 2000 ps, all simulations can be performed in parallel, which makes these techniques more efficient. This parallelization is an advantage that may not be underestimated, despite the observation that all considered enhanced sampling techniques yield almost similar results in the description of the reactant side (up to TS). This is in contrast with earlier work of the authors, where the MTD method was preferred over US [108]. This was due to the fact that MTD requires less prior knowledge on the reaction path, which is not a restricting factor for the reaction under study here.

Given the selected parameters for the US and TI simulations, the former technique leads to a lower error on the resulting free energy profile (see Section 5 of the ESI). Therefore, we will select US as the most suitable enhanced sampling technique for the reaction under study. A similar conclusion was made by an earlier

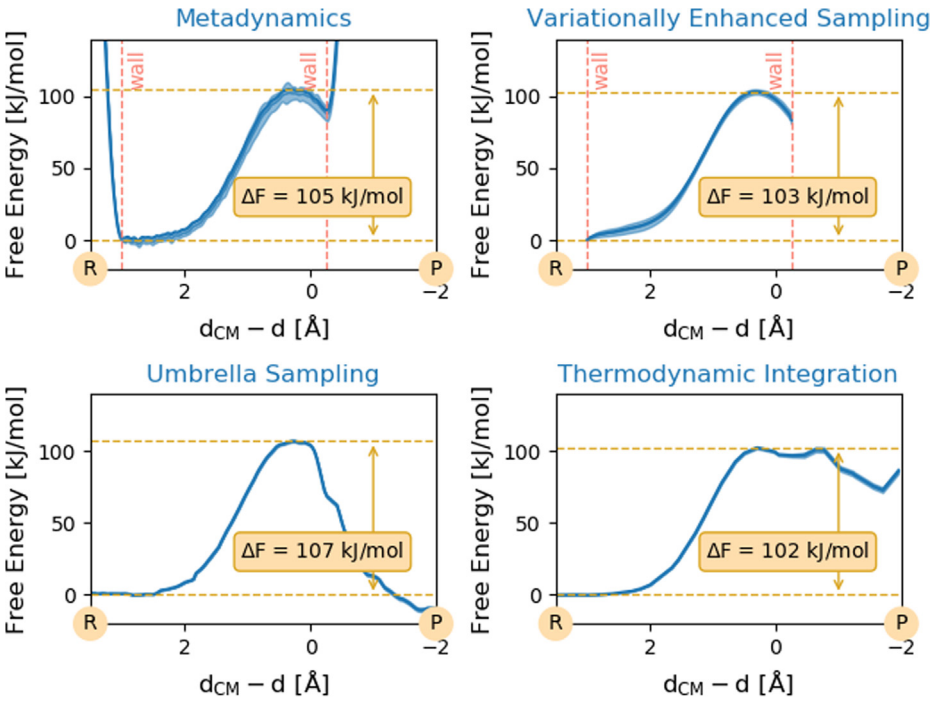

Fig. 3. Free energy profiles and error bars at 623 K in function of the one-dimensional collective variable 1D-DI obtained with different enhanced sampling methods. Furthermore, the forward barrier is shown on the graphs for each method. The reactant (R) and product (P) side of the reaction are also indicated. The error estimation is discussed in Section 5 of the ESI.

benchmark study where force fields were used to compare the efficiency of enhanced sampling techniques in the construction of free energy profiles for breathing metal–organic frameworks [43]. Nevertheless, it should be noted that this choice largely depends on the system under study.

3.2. The influence of the collective variable on the intrinsic barrier

The specific nature of the reaction under study (methylation of ethene in H-ZSM-5) requires preferentially the introduction of a two-dimensional set of collective variables. Several choices of collective variables have been proposed in Fig. 1 to describe the reaction. The first type consists of coordination numbers (CNs) which are able to describe the breaking and formation of the C-O and C-C bond [4,101,102]. The second type of CVs consists of distances between the atoms of the breaking and forming bonds. Two-dimensional free energy surfaces are constructed within the US protocol, as this technique is selected as the most appropriate method for the envisaged application in this work. The choice of the two-dimensional windows is reported in Table S4 of the ESI.

Fig. 4 displays the resulting FESs for the two types (DI and CN) of collective variables. Obviously, the shape of the interesting regions of the FES differs substantially with the type of the CVs. The reactant and product valley are uniquely described in the two dimensional FES. The two basins are well separated, illustrating that the two types (DI and CN) of collective variables are well chosen. The reactant region does not overlap with the basin of attraction of the products. However, each of the CVs does not act as a good reaction coordinate if we consider them separately. On the other hand, a suitable linear combination of CV1 and CV2 can result in an appropriate reaction coordinate. A one-dimensional free energy profile $F_q(q)$ can easily be extracted by integration of the 2D probability distribution as outlined in Section 2.4.2, but for this dimensionality reduction we need an appropriate choice of $q(CV1, CV2)$. This choice is not trivial, and depends on the shape of the interesting region of the 2D-FES. The 2D-FES belonging to type DI suggests to introduce $q = d_{CM}$-d, which has already proven its success in earlier works of the authors [77,108,109]. This results into the 1D free energy profile displayed in the right panel (yellow curve) of Fig. 5. If we perform an independent enhanced simulation along $q = d_{CM}$-d as one-dimensional reaction coordinate (1D-DI), we get a free energy profile (orange curve in the right panel of Fig. 5), which perfectly coincides with the profile obtained after 2D → 1D projection. This is not a coincidence, but rather an indication that $q = d_{CM}$-d is indeed a suitable reaction coordinate for this specific reaction. Analogously, the left panel of Fig. 5 shows the free energy profile after projecting the 2D-FES surface belonging to type CN to the 1D reaction coordinate $q = CN_{CC} - CN_{OC}$. In this case, the profile cannot be reproduced in an independent simulation in which sampling occurs along the one-dimensional $q = CN_{CC} - CN_{OC}$ as collective variable, as the US simulations do not reach convergence.

The plots in Fig. 5 clearly show that the free energy profiles in terms of the various collective variables have not only different shapes but also different barriers if they are determined by the free energy difference between the maximum and the minimum of the profile as done in earlier work [77]. For Type CN a barrier of ± 127 kJ/mol is observed, while for the type DI collective variables the barrier is systematically lower and amounts to 102–107 kJ/mol.

To enable direct comparison of the free energy profiles obtained by sampling in different collective variable spaces, the transformations defined in Section 2.4.2 need to be applied. From here on, we will distinguish between the collective variable in which the sampling is performed during the simulation, labeled Q_{SAM}, and the collective variable Q_{REP} which represents the reaction coordinate in which the free energy profile is plotted. Q_{REP} does not necessarily coincide with Q_{SAM}, as a transformation of the free energy profile can be performed.

To illustrate, the type DI profiles, displayed in Fig. 5, can be transformed to the space spanned by the one-dimensional $q = CN_{CC}$-CN_{OC} reaction coordinate. The resulting plot is shown in the left

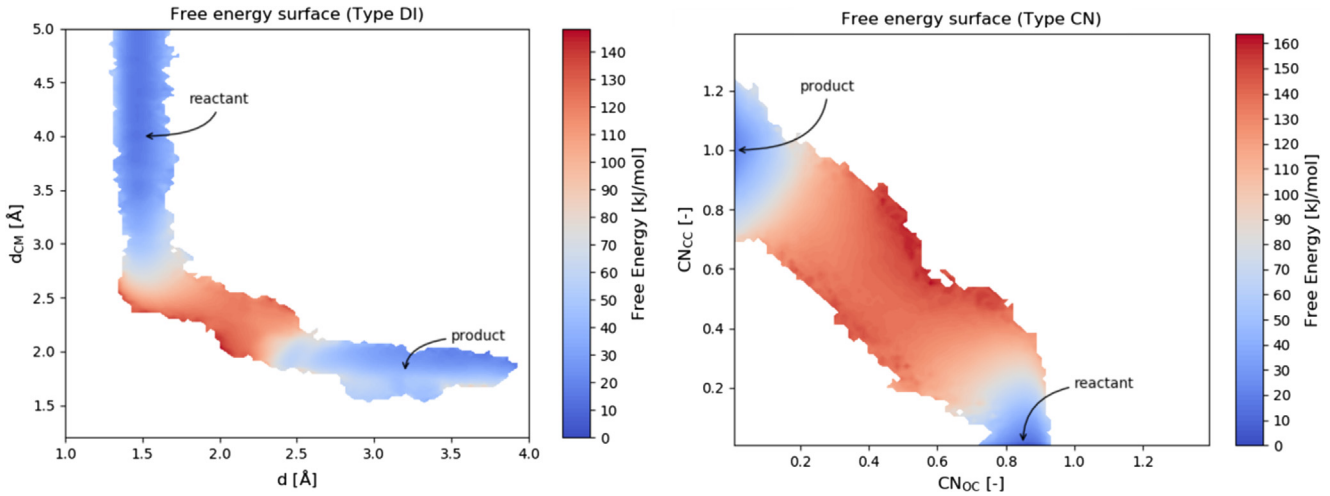

Fig. 4. Two-dimensional free energy surfaces as a function of the distances d_{CM} and d (left panel), and as a function of the coordination numbers CN_{CC} and CN_{OC} as collective variables (right panel).

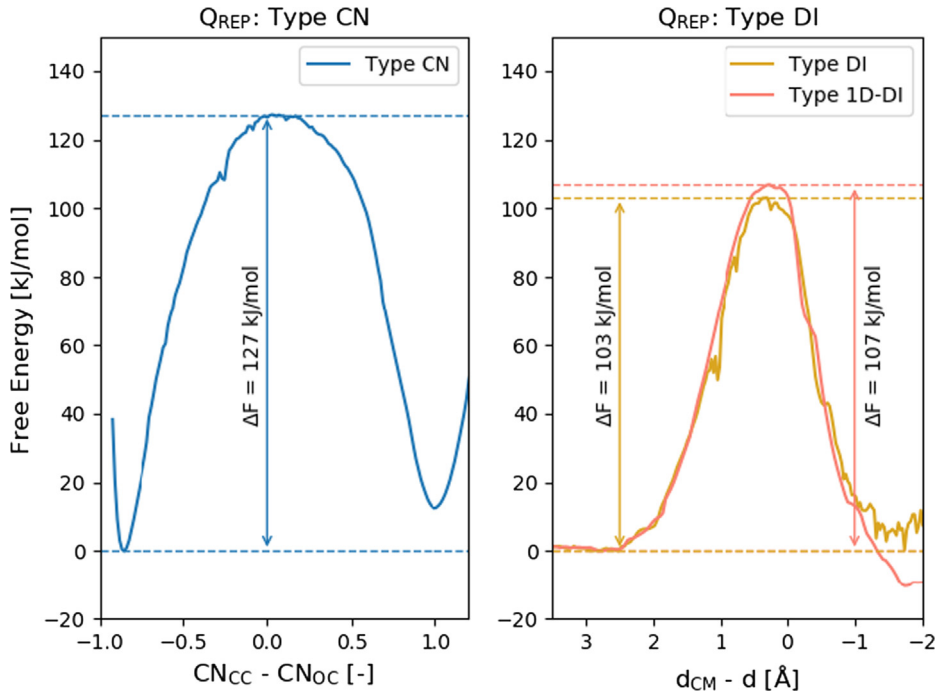

Fig. 5. Free energy profiles at 623 K obtained by projecting the 2D-FES of Fig. 4 onto a 1D space. The left panel displays the 2D → 1D reduction in the space of collective variables of Type CN (blue curve). The right panel shows the 2D → 1D reduction in the space of collective variables of Type DI (yellow curve). The orange curve is the energy profile resulting from an independent sampling of the space along the one-dimensional q = d_{CM} – d (1D-DI) as reaction coordinate. The forward free energy barriers are also reported on the figures.

panel of Fig. 6. Obviously, the two $F_{CN}(CN_{CC}\text{-}CN_{OC})$ free energy profiles (yellow and orange curves) are almost similar with each other. Both are deduced from the free energy profiles $F_{DI}(d_{CM} - d)$, represented by the two curves in the right panel of Fig. 5. Interestingly, the shape of the transformed profiles nicely coincides with the original free energy profile, obtained after sampling in the 2D coordination number space. This behavior points toward a clear consistency of our numerical results, giving evidence that the different sampling simulations have been performed accurately and that the simulation times have been respected sufficiently long to get convergence. The accuracy of the transformed energy profile depends on the conditional probability $p_{2|1}(CN_{OC}, CN_{CC}|d_{CM} - d)$ or $p_{2|1}(CN_{OC}, CN_{CC}|d, d_{CM})$, which should be extracted from the 1D or 2D simulations, and which turns out to be correctly sampled.

A similar protocol is applied for the free energy profiles in the right panel of Fig. 6. The blue profile results originally from the 2D-FES as a function of the coordination numbers CN_{CC} and CN_{OC} as collective variables (Fig. 4). After a 2D → 1D projection a CV transformation CN → DI has been performed, resulting to the blue curve of the right panel of Fig. 6.

It is important to note that the free energy profiles between the reactant valley and the transition state region all coincide quite nicely, after applying the transformations. The most accurate plot should correspond with the profile expressed in the same CV space,

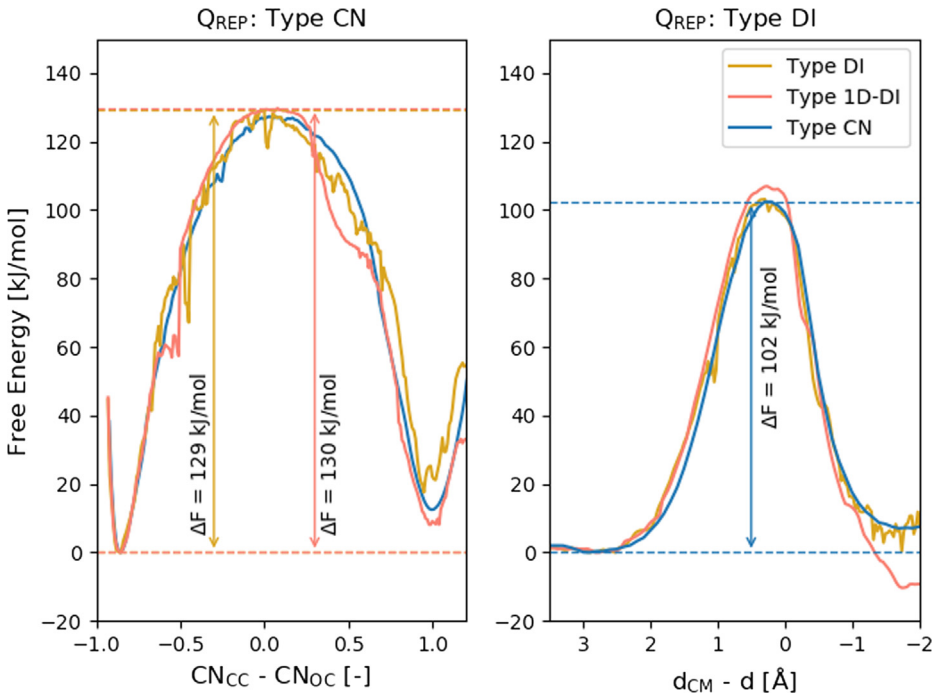

Fig. 6. Free energy profiles at 623 K obtained after applying transformations between the two types of collective variables. The left panel displays the transformation $F_{DI}(d_{CM} - d) \rightarrow F_{CN}(CN_{CC}\text{-}CN_{OC})$ (yellow and orange curves), while the right panel shows the reverse transformation $F_{CN}(CN_{CC}\text{-}CN_{OC}) \rightarrow F_{DI}(d_{CM} - d)$ (blue curve), starting from $F_{CN}(CN_{CC}\text{-}CN_{OC})$ of Fig. 5, which represents the 2D → 1D reduction in the space of collective variables of Type CN. The forward free energy barriers are also reported on the figures.

wherein the sampling has been accomplished. The product region is not always correctly reproduced. However, if the sampling has been performed sufficiently long as is suggested by the nice overall reproduction of the energy profiles, one could expect that the product region should also be reproduced consistently. The discrepancy is inherently related to the rather unstable carbocations formed after the methylation, which transform into various intermediates, such as propene, cyclopropane, propoxide, propanol... As a result, the product region is not equally well sampled in the various simulations. We will no longer focus on this issue since this is not the scope of this work.

There are some interesting features regarding the shape of the profiles which require some attention. The $F(CN_{CC} - CN_{OC})$ profile shows a thin well for the reactants, predicted by all the types of CVs, while in the $F(d_{CM} - d)$ profiles a broad range of configurations is observed. This can partly be ascribed to the way a coordination number is related to the bond distance, as given in Eq. (1). In the reactant valley the distance d is of the order of 1 Å, giving a coordination number of $CN_{OC} \cong 1$, while the distance between methanol and ethene (reflected by d_{CM}) can amount to several Ångström, without affecting the value of the coordination number CN_{CC} (see Figure S14), which remains zero, as is further illustrated by the mobility plots of methanol and ethene in the reactant state (Figure S15). In the enhanced sampling simulations using coordination numbers as collective variables (Type CN) we observe a large mobility of the ethene molecule. This is reflected into a broad valley of distances d_{CM}-d after transformation from the coordination number space to the distance space, as the free energy relates to the probability to sample a particular state.

Summarizing, different collective variables may be used to model a reaction, which, in principle, all lead to specific free energy profiles. However, if the CV space is sufficiently sampled, they are all exactly reproduced by applying a proper transformation. In the next section, we further use this knowledge to describe the reaction kinetics properly.

Summarizing, different collective variables may be used to model a reaction, which, in principle, all lead to specific free energy profiles. However, if the CV space is sufficiently sampled, they are all exactly reproduced by applying a proper transformation. In the next section, we further use this knowledge to describe the reaction kinetics properly.

3.3. Reaction kinetics

Previous analysis suggests that the configurational freedom in the reactant and transition state should be properly accounted for when calculating reaction rates. This can be done by defining transition rates instead of free energy barriers to compare the speed of different reactions, independently of the chosen collective variables. We follow the procedure as outlined in the Appendix and discussed in more details in Section 11 of the ESI.

As a final result, the forward transition-state rate constant can be written as :

$$k_{R\rightarrow P}^{TST} = A\frac{e^{-\beta\Delta F_{q_R\rightarrow q^{\ddagger}}}}{\int_{q_R}^{q^{\ddagger}} e^{-\beta F(q)}dq}$$

with a prefactor $A = \left(\frac{k_B T}{2\pi}\right)^{1/2}\left\langle Z^{1/2}\right\rangle_{q=q^{\ddagger}}$

with the inverse mass Z of the reaction coordinate.

The computation of the term $\Delta F_{q_R\rightarrow q^{\ddagger}}$ can be obtained from enhanced MD techniques such like Umbrella Sampling (US), Metadynamics (MTD), etc. All free energies are regarded as relative with respect to the reference reactant state corresponding to q_R. In this work, the free energy profile is computed within the Umbrella Sampling protocol and $\Delta F_{q_R\rightarrow q^{\ddagger}}$ is then determined by the maximum – minimum difference.

The prefactor A is expressed in terms of the average of the square of the inverse mass of the reaction coordinate or its gradi-

ent, which in turn is related to the rate of change of the collective variable, evaluated at the transition state. Although the expression for the prefactor A indicates that a molecular simulation needs to be performed in which the system is constrained to be in the exact transition state ($q = q^{\ddagger}$), this is not necessarily required. The prefactor can also be estimated from a molecular simulation which is instead biased by a certain bias potential $U_b(q)$ (for example during Umbrella Sampling). More details are given in in Section 11 of the ESI. Finally, the denominator $\bar{Z}_R = \int_{q_R}^{q^{\ddagger}} e^{-\beta F(q)} dq$ is proportional to the partition function of the reactant and yields information on the width and depth of the free energy profile in terms of the collective variable in the reactant region. We computed the rate constants according to this equation for the methylation reaction and investigated the influence of the choice of the collective variable. As stated earlier, the enhanced sampling simulations were performed using the various collective variable(s). Table 1 tabulates the rate constants for various combinations of Q_{SAM} and Q_{REP}. The meaning of this notation has been explained earlier (Section 3.2). Each row reports the rate constants derived from MD simulations based on the same type of collective variables.

All reaction rate constants are differing at most by one order of magnitude, [20] even though the free energy barrier $\Delta F_{q_R \rightarrow q^{\ddagger}}$ obtained by subtracting the minimum from the maximum free energy, was itself dependent on the chosen collective variable as illustrated in Table S6 of the ESI. Since the rate constant represents a macroscopically measurable quantity, it should indeed be independent of the way we describe it microscopically. Therefore, one cannot simply rely on the free energy barrier to make statements on how fast a reaction will occur. Instead, one needs to compute all contributions to the reaction rate consistently. By calculating the rate expression, we also account for the width and the depth of various parts of the $F(q)$ profile. Finally, the impact of Q_{SAM}, the CV used to perform the enhanced sampling, can also readily be extracted from Table 1, by examining the reaction rates belonging to a single column. The influence is also rather limited, indicating that each CV succeeds in a correct description of the reaction and associated reaction rate.

By comparing the formula for the reaction rate with the Eyring-Polanyi equation [110], a phenomenological free energy barrier $\Delta F^{\ddagger}$ can be introduced, as was done earlier by Bučko et al. [111] and the current authors: [108]

$$\Delta F^{\ddagger} = \Delta F_{q_R \rightarrow q^{\ddagger}} + k_B T \ln\left(\frac{k_B T \bar{Z}_R}{hA}\right)$$

The resulting values are summarized in Table 2, and surprisingly they are very similar within a range of 10%. We may conclude that the phenomenological free energy barrier associated to a chemical process, which in this example stands for the methylation of ethene in H-ZSM-5, represents a quantity which is independent of the choice of the collective variable used during sampling (Q_{SAM}) of the configuration space. It is a more correct and physical representation of a barrier than the difference between maximum and minimum on a free energy profile along a certain collective variable, which largely depends on the choice of this last coordinate, as demonstrated in this paper.

To test the reliability of the results, they are submitted to a committor analysis in Section 12 of the ESI. The committor histograms corresponding to the transition state expressed in the space of a collective variable of Type 1D-DI and of Type CN (CN_{CC}-CN_{OC}) are shown in Figure S10 and S11 respectively. They are clearly peaked at $p_P(q) = 0.5$, confirming the quality of the selected collective variable. Furthermore, a molecular dynamics simulation is performed using the obtained free energy profile as a bias, as discussed in Section 13 of the ESI.

Table 1
Reaction rate constant k (in 1/s) at 623 K from the US simulations employing different collective variables.

	Q_{REP}	
Q_{SAM}	CN_{CC} - CN_{OC}	d_{CM} - d
Type CN	1.58 10^3	2.86 10^3
Type DI	1.13 10^3	1.04 10^4
Type 1D-DI	9.74 10^2	5.48 10^3

Table 2
Phenomenological free energy barrier (in kJ/mol) at 623 K.

	Q_{REP}	
Q_{SAM}	CN_{CC} - CN_{OC}	d_{CM} - d
Type CN	118.3	115.2
Type DI	120.0	108.5
Type 1D-DI	120.8	111.8

3.4. Comparison to theoretical and experimental literature data

Reliable intrinsic rates and free energy barriers could be obtained irrespective of the collective variable. At this moment, it is instructive to compare the here obtained rates and free energies with earlier literature data. The methylation of ethene in H-ZSM-5 has been the topic of various comparative studies [17,19,20] with experimental kinetic data [21,22]. Experimentally, one obtains apparent rates, which are in this case referred to the state where methanol is adsorbed on the Brønsted acid site while ethene is still in the gas phase. Indeed, the reaction was determined to be zeroth order with respect to methanol and first order with respect to ethene [21,22] and could be described by the following rate equation:

$$r = k p^0_{methanol} p^1_{ethene}$$

with $p_{methanol}$ and p_{ethene} the partial pressures of methanol and ethene. The reaction rate constants obtained here with the MD approach correspond to intrinsic kinetics where all reactants, thus methanol and ethene, are adsorbed on the zeolite. These values cannot directly be compared with experiment. However, in ref [17] also intrinsic rates were reported using at that time a rigid rotor harmonic oscillator model and a finite cluster model consisting of 46 T atoms. At the ONIOM(B3LYP/6–31 + g(d):HF/6–31 + g(d))-D//ONIOM(B3LYP/6–31 + g(d):MNDO) level of theory a value of 5.5 10^3 s^{-1} at 623 K for k_{int} was obtained, which is in very good agreement with the values obtained here (Table 1).

It is however interesting to also compare with the values of Svelle et al. [19] and Piccini et al. [20]. Svelle et al. used a composite scheme to obtain apparent enthalpy barriers with chemical accuracy, whereas Piccini et al. used anharmonic corrections to get better estimates of the pre-exponential factor. In previous methods, no molecular dynamics simulations were done to sample the configurational space. A direct comparison with the values of Svelle and Piccini is hampered as they did not report intrinsic free energy barriers or intrinsic reaction rates. This makes a direct comparison very difficult, as there are no generally accepted methodologies to extract enthalpic barriers and adsorption enthalpies from ab initio molecular dynamics methods. To enable a comparison with experimental data and earlier theoretical data, we calculated the co-adsorption free energy for ethene $\Delta G_{ads,ethene}$ from static periodic

DFT calculations and determined the apparent rate constant k_{app} based on the equilibrium constant K_1 as: [112]

$$k_{app} = K_1 k_{int}$$

This formula is derived in Section 14 of the ESI. The two adsorbed complexes [Z-H,CH_3OH(ads),ethene(g)] and [Z-H,CH_3OH (ads), ethene(ads)] are in equilibrium determined by the equilibrium constant:

$$K_1 = V_0 \exp(-\frac{\Delta G_{ads,ethene}}{RT})$$

with V_0 the molar volume of an ideal gas which equals 0.0518 m^3/mol at 623 K and 1 atm, R the gas constant and introducing the co-adsorption free energy $\Delta G_{ads,ethene}$ of ethene as illustrated in Fig. 7 and further discussed in Section S14 of the ESI.

The computation of adsorption energies is always very sensitive to the selected level of theory and dispersion scheme. Large variations are common practice in this field. To reliably estimate the spread on the adsorption energies, we performed single point energy calculations with a whole set of functionals and dispersion schemes frequently used in literature [48,75] starting from optimized structures obtained using revPBE-D3 (see Section S14 of the ESI). Co-adsorption electronic energies are found in the range of −11 to −37 kJ/mol , thus corresponding quite well with the experimental co-adsorption enthalpies of −24 to −31 kJ/mol [19,113]. For the two extreme values, apparent reaction rate constants are listed in Table 3, containing both the results corresponding to the revPBE-D3 and the hybrid B3LYP-D3 level of theory.

The difference in the co-adsorption free energy running up to 25 kJ/mol leads to two orders of magnitude variation in the equilibrium constant, indicating that prudence is required in making conclusions when assessing apparent kinetics extracted from intrinsic rate constants. Nevertheless we take note that the experimental value of 1.95 10^{-4}(mbar s)$^{-1}$[18] is close to the theoretically proposed range of values (see Table 3). Looking more closely to the revPBE-D3 results, which are used in both the static as the dynamic simulations, values ranging from 2.94 10^{-3} to 3.14 10^{-2} (mbar s)$^{-1}$ are attained, on the verge of kinetic accuracy.

The results discussed here thus show that by combining static and enhanced sampling methodologies, one can almost attain kinetic accuracy, although the selection of DFT functional and dispersion scheme remains a crucial factor in the finally attained accuracy. As such, further testing and benchmarking of both static and enhanced sampling methodologies for zeolite catalysis remain essential for the development of a generally applicable quantum mechanical methodology.

4. Conclusion

The methylation of ethene in H-ZSM-5, a crucial reaction in the MTO process, was thoroughly investigated with enhanced sampling MD techniques. The methylation reaction is one of the best characterized reactions in zeolite science, both from a theoretical and experimental viewpoint. In this work we presented a protocol to describe the reaction kinetics, independent of the choice of the collective variable(s) representing the reaction coordinate and the enhanced sampling technique.

First, the forward intrinsic methylation free energy barrier was calculated using four enhanced sampling techniques, namely metadynamics, variationally enhanced sampling, umbrella sampling and thermodynamic integration (or umbrella integration). The four different methodologies give similar results, although some have (dis)advantages compared to others, depending on the specific reaction type. A unique protocol making use of the most appropriate techniques cannot be proposed. For the methylation reaction of ethene, the MTD and VES techniques require the introduction of walls to limit the sampling to the region of interest, which is not trivial without prior knowledge of the specific reaction path. Umbrella sampling was selected as the most appropriate technique to study the methylation of ethene, thanks to its low error bar.

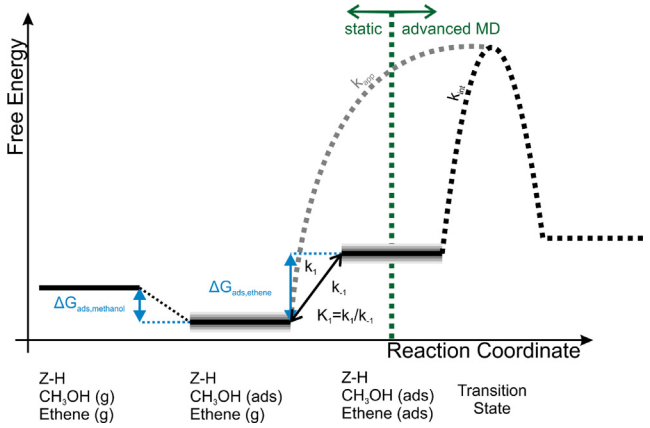

Fig. 7. Schematic representation of the relation between apparent and intrinsic kinetics. For the calculation of $\Delta G_{ads,ethene}$ various schemes are used, shown by the grey uncertainty in the co-adsorption step of ethene. The value of k_{int} is obtained dynamically in this work.

In the second part, the influence of the chosen collective variable on the intrinsic free energy barrier was examined. Therefore, three types of collective variables were proposed which could differentiate between the reactant, transition and product state of the methylation reaction under study. We have proven the importance of transformations between different collective variable spaces. Nevertheless, the free energy profile typically still depends on the collective variable(s) used to represent the reaction coordinate. A collective variable invariant measure is necessary for enhanced sampling to be competitive with static methodologies. Therefore, the importance of accounting for the configurational freedom in the reactant state, when calculating free energy barriers from enhanced sampling simulations, was demonstrated. We showed that by calculating reaction rates and phenomenological free energy barriers, reliable estimates for the intrinsic kinetics can be obtained which are nearly independent on the choice of the collective variable.

Finally, we validated our intrinsic reaction rate constants by comparison with theoretical and experimental data available in literature. Our data correspond very well with the intrinsic reaction rate constant of 5.5 10^3 1/s at 623 K, reported by Van Speybroeck et al. [17] Direct comparison with other theoretical work and experimental work was impeded, as only apparent rates were reported in literature. Apparent kinetics were related with intrinsic kinetics extracted from the advanced MD simulations by the equilibrium constant for the co-adsorption of ethene which was calculated using static DFT approaches. Taking into account a whole set of functionals and dispersion schemes, a range of apparent rate constants were extracted, approaching the experimental value of 1.95 10^{-4} (mbar.s)$^{-1}$. When consequently using the revPBE-D3 level of theory in both the static and enhanced sampling simulations, kinetic coefficients with near chemical accuracy were obtained.

The results presented in this work show that ab initio enhanced sampling techniques have the potential to yield valuable insights when describing chemical reactions in a complex molecular environment. Nevertheless, ab initio molecular dynamics simulations are computationally expensive, making it difficult to use them as stand-alone methods. Therefore, further exploration of enhanced

Table 3
Apparent reaction rate constants k_{app} at 623 K for the methylation of ethene, calculated based on the smallest and highest estimate for the intrinsic rate constants k_{int} (see Table 1). Four level of theories are considered for the calculation of the co-adsorption free energy of ethene $\Delta G_{ads,ethene}$ (see Table S11 of the ESI): revPBE-dDsC (lower limit) [114,115], revPBE-D3, B3LYP-D3 and vdW-DF (upper limit) [116,117].

	Lower limit	B3LYP-D3	revPBE-D3	Upper limit	Lower limit	B3LYP-D3	revPBE-D3	Upper limit	exp
k_{int}	9.74 10^{2}				1.04 10^{4}				
$\Delta E_{ads,ethene}$[kJ/mol]	−11.0	−20.3	−22.7	−36.8	−11.0	−20.3	−22.7	−36.8	−24 – −31 [17,121]
$\Delta G_{ads,ethene}$[kJ/mol]	41.7	32.5	30.1	16.0	41.7	32.5	30.1	16.0	
K_1[m^3/mol]	1.64 10^{-5}	9.75 10^{-5}	1.57 10^{-4}	2.35 10^{-3}	1.64 10^{-5}	9.75 10^{-5}	1.57 10^{-4}	2.35 10^{-3}	
k_{app}[m^3/(mol.s)]	1.60 10^{-2}	9.50 10^{-2}	1.52 10^{-1}	2.28	1.71 10^{-1}	1.01	1.63	2.44 10^{1}	
k_{app}[1/mbar.s)]	3.08 10^{-4}	1.83 10^{-3}	2.94 10^{-3}	4.41 10^{-2}	3.29 10^{-3}	1.96 10^{-2}	3.14 10^{-2}	4.71 10^{-1}	1.9510^{-4} [18]

sampling techniques combined with static methodologies is of utmost importance for their general application.

Declaration of Competing Interest

The authors declared that there is no conflict of interest.

Acknowledgements

We acknowledge the Fund for Scientific Research - Flanders (FWO), the Research Board of Ghent University (BOF) and funding from the European Union's Horizon 2020 research and innovation program (consolidator ERC grant agreement No 647755 – DYNPOR (2015-2020)). K.D. acknowledges the FWO for her predoctoral fellowship. The computational resources and services used were provided by Ghent University (Stevin Supercomputer Infrastructure) and the VSC, Belgium (Flemish Supercomputer Center), funded by the Research Foundation - Flanders (FWO).

Appendix A:

Transition state theory allows to derive an expression for the rate of a reaction $R \rightarrow P$ based on the definition of the transition state as a dividing surface separating the reactants (R) from the products (P).[118–121] The theory is based on some key assumptions among which: (1) thermodynamic equilibrium must prevail throughout the entire system for all degrees of freedom and (2) any trajectory crossing the dividing surface will not turn back to the reactant valley or recross the dividing surface. The expression for the transition-state rate constant for the reaction R → P can be written as: [38,111,122,123]

$$k_{R\rightarrow P}^{TST} = \frac{\langle \dot{q}\,\theta(\dot{q})\,\delta(q-q^{\ddagger})\rangle}{\langle \theta(q^{\ddagger}-q)\rangle}$$

Herein, q represents the reaction coordinate and is a function of the molecular configuration $q \equiv Q(\mathbf{r}^N)$. $q^{\ddagger}$ represents the value of the reaction coordinate at the transition state. The population of the reactant is given by the step function $\theta(q^{\ddagger}-q)$ with his associated flux $\dot{\theta}(q-q^{\ddagger}) = \dot{q}\,\delta(q-q^{\ddagger})$. $\dot{q}$represents the velocity associated to the reaction coordinate. <. . .> is an equilibrium average over the canonical distribution function $e^{-\beta H(\mathbf{r}^N,\mathbf{p}^N)}$where H is the system Hamiltonian and $\beta = 1/k_BT$.

Integration over the velocities leads to [61,124] :

$$k_{R\rightarrow P}^{TST} = \left(\frac{k_BT}{2\pi}\right)^{1/2} \frac{\int \delta(q^{\ddagger}-q(\mathbf{x}^N))\left|\vec{\nabla}_x q\right| e^{-\beta U(\mathbf{x}^N)} d\mathbf{x}^N}{\int_R e^{-\beta U(\mathbf{x}^N)} d\mathbf{x}^N}$$

with the mass-weighted coordinates $\mathbf{x}_i = \sqrt{m_i}\,\mathbf{r}_i$. This expression is equivalent with the more familiar form [61,124] :

$$k_{R\rightarrow P}^{TST} = \left(\frac{k_BT}{2\pi}\right)^{1/2} \frac{\left\langle Z^{1/2}\,\delta(q^{\ddagger}-q)\right\rangle_r}{\langle \theta(q^{\ddagger}-q)\rangle_r}$$

The full elaboration is outlined in Section S11. Z represents the inverse mass of the reaction coordinate:

$$Z = \sum_{i=1}^{N} \frac{1}{m_i} \sum_{\mu=x,y,z} \frac{\partial q}{\partial r_{i,\mu}} \frac{\partial q}{\partial r_{i,\mu}}$$

and the notation $\langle\rangle_r$ means an average over configurational coordinates only.

$\frac{\langle \delta(q^{\ddagger}-q)\rangle_r}{\langle \theta(q^{\ddagger}-q)\rangle_r}$ represents the probability $P(q^{\ddagger})$ that the system is at $q^{\ddagger}$ normalized by the reactant density. Remark that the norm $\left|\vec{\nabla}_x q\right|$ is equivalent with $Z^{1/2}$.

It is convenient to introduce some reference value q_R of the reaction coordinate characteristic for the reactant state [111]. The free energy needed to shift the reaction coordinate from the value of q_R to $q^{\ddagger}$ is then given by :

$$\Delta F_{q_R\rightarrow q^{\ddagger}} = -k_BT \ln\left[\frac{P(q^{\ddagger})}{P(q_R)}\right]$$

The forward transition-state rate constant can be rewritten as :

$$k_{R\rightarrow P}^{TST} = \left(\frac{k_BT}{2\pi}\right)^{1/2} \left\langle Z^{1/2}\right\rangle_{q=q^{\ddagger}} P(q_R)\, e^{-\beta \Delta F_{q_R\rightarrow q^{\ddagger}}}$$

or

$$k_{R\rightarrow P}^{TST} = A \frac{e^{-\beta \Delta F_{q_R\rightarrow q^{\ddagger}}}}{\int_{q_R}^{q^{\ddagger}} e^{-\beta F(q)} dq}$$

as $P(q_R) = \frac{\langle \delta(q_R-q)\rangle_r}{\langle \theta(q^{\ddagger}-q)\rangle_r} = \frac{1}{\int_{q_R}^{q^{\ddagger}} e^{-\beta F(q)} dq}$ (F(q_R) = 0 at the reference)

with a prefactor $A = \left(\frac{k_BT}{2\pi}\right)^{1/2} \left\langle Z^{1/2}\right\rangle_{q=q^{\ddagger}}$

The computation of the term $\Delta F_{q_R\rightarrow q^{\ddagger}}$can be obtained from the blue moon ensemble method [61,122] but also from other enhanced MD techniques such like Umbrella Sampling (US), Metadynamics (MTD), etc. All free energies are regarded as relative with respect to the reference reactant state corresponding to q_R. In this work the free energy profile is computed within the Umbrella Sampling protocol and $\Delta F_{q_R\rightarrow q^{\ddagger}}$ is then determined by the maximum – minimum difference.

Appendix B. Supplementary material

Supplementary data to this article can be found online at https://doi.org/10.1016/j.jcat.2020.04.015.

References

[1] V. Van Speybroeck, K. Hemelsoet, L. Joos, M. Waroquier, R.G. Bell, C.R.A. Catlow, Advances in theory and their application within the field of zeolite chemistry, Chem. Soc. Rev. 44 (2015) 7044–7111.

[2] F. Pietrucci, Strategies for the exploration of free energy landscapes: Unity in diversity and challenges ahead, Rev. Phys. 2 (2017) 32–45.
[3] N. Hansen, W.F. van Gunsteren, Practical aspects of free-energy calculations: a review, J. Chem. Theory Comput. 10 (2014) 2632–2647.
[4] V. Van Speybroeck, K. De Wispelaere, J. Van der Mynsbrugge, M. Vandichel, K. Hemelsoet, M. Waroquier, First principle chemical kinetics in zeolites: the methanol-to-olefin process as a case study, Chem. Soc. Rev. 43 (2014) 7326–7357.
[5] K. De Wispelaere, S. Bailleul, V. Van Speybroeck, Towards molecular control of elementary reactions in zeolite catalysis by advanced molecular simulations mimicking operating conditions, Catal. Sci. Technol. 6 (2016) 2686–2705.
[6] L. Grajciar, C.J. Heard, A.A. Bondarenko, M.V. Polynski, J. Meeprasert, E.A. Pidko, P. Nachtigall, Towards operando computational modeling in heterogeneous catalysis, Chem. Soc. Rev. 47 (2018) 8307–8348.
[7] M.W. Erichsen, K. De Wispelaere, K. Hemelsoet, S.L.C. Moors, T. Deconinck, M. Waroquier, S. Svelle, V. Van Speybroeck, U. Olsbye, How zeolitic acid strength and composition alter the reactivity of alkenes and aromatics towards methanol, J. Catal. 328 (2015) 186–196.
[8] W.L. Dai, C.M. Wang, M. Dyballa, G.J. Wu, N.J. Guan, L.D. Li, Z.K. Xie, M. Hunger, Understanding the early stages of the methanol-to-olefin conversion on H-SAPO-34, ACS Catal. 5 (2015) 317–326.
[9] K. De Wispelaere, C.S. Wondergem, B. Ensing, K. Hemelsoet, E.J. Meijer, B.M. Weckhuysen, V. Van Speybroeck, J. Ruiz-Martinez, Insight into the effect of water on the methanol-to-olefins conversion in H-SAPO-34 from molecular simulations and in situ microspectroscopy, ACS Catal. 6 (2016) 1991–2002.
[10] I. Yarulina, S. Bailleul, A. Pustovarenko, J.R. Martinez, K. De Wispelaere, J. Hajek, B.M. Weckhuysen, K. Houben, M. Baldus, V. Van Speybroeck, F. Kapteijn, J. Gascon, Suppression of the aromatic cycle in methanol-to-olefins reaction over ZSM-5 by post-synthetic modification using calcium, ChemCatChem 8 (2016) 3057–3063.
[11] I. Yarulina, K. De Wispelaere, S. Bailleul, J. Goetze, M. Radersma, E. Abou-Hamad, I. Vollmer, M. Goesten, B. Mezari, E.J.M. Hensen, J.S. Martinez-Espin, M. Morten, S. Mitchell, J. Perez-Ramirez, U. Olsbye, B.M. Weckhuysen, V. Van Speybroeck, F. Kapteijn, J. Gascon, Structure-performance descriptors and the role of Lewis acidity in the methanol-to-propylene process, Nat. Chem. 10 (2018) 804–812.
[12] R.Y. Rohling, E. Uslamin, B. Zijlstra, I.C. Tranca, N.A.W. Filot, E.J.M. Hensen, E.A. Pidko, An active alkali-exchanged faujasite catalyst for p-Xylene production via the one-pot diels-alder cycloaddition/dehydration reaction of 2,5-dimethylfuran with ethylene, ACS Catal. 8 (2018) 760–769.
[13] C. Wang, Y.Y. Chu, J. Xu, Q. Wang, G.D. Qi, P. Gao, X. Zhou, F. Deng, Extra-framework aluminum-assisted initial c-c bond formation in methanol-to-olefins conversion on zeolite H-ZSM-5, Angew. Chemie-Int. Ed. 57 (2018) 10197–10201.
[14] M.E.Z. Velthoen, S. Nab, B.M. Weckhuysen, Probing acid sites in solid catalysts with pyridine UV-Vis spectroscopy, PCCP 20 (2018) 21647–21659.
[15] S. Bailleul, I. Yarulina, A.E.J. Hoffman, A. Dokania, E. Abou-Hamad, A.D. Chowdhury, G. Pieters, J. Hajek, K. De Wispelaere, M. Waroquier, J. Gascon, V. Van Speybroeck, A supramolecular view on the cooperative role of bronsted and lewis acid sites in zeolites for methanol conversion, J. Am. Chem. Soc. 141 (2019) 14823–14842.
[16] V. Van Speybroeck, K. Van Cauter, B. Coussens, M. Waroquier, Ab initio study of free-radical polymerizations: cost-effective methods to determine the reaction rates, ChemPhysChem 6 (2005) 180–189.
[17] V. Van Speybroeck, J. Van der Mynsbrugge, M. Vandichel, K. Hemelsoet, D. Lesthaeghe, A. Ghysels, G.B. Marin, M. Waroquier, First principle kinetic studies of zeolite-catalyzed methylation reactions, J. Am. Chem. Soc. 133 (2011) 888–899.
[18] C.R.A. Catlow, Prediction of rate constants for catalytic reactions with chemical accuracy, Angew. Chemie-Int. Ed. 55 (2016) 9132–9133.
[19] S. Svelle, C. Tuma, X. Rozanska, T. Kerber, J. Sauer, Quantum chemical modeling of zeolite-catalyzed methylation reactions: toward chemical accuracy for barriers, J. Am. Chem. Soc. 131 (2009) 816–825.
[20] G. Piccini, M. Alessio, J. Sauer, AbInitio calculation of rate constants for molecule-surface reactions with chemical accuracy, Angew. Chemie-Int. Ed. 55 (2016) 5235–5237.
[21] S. Svelle, P.A. Ronning, S. Kolboe, Kinetic studies of zeolite-catalyzed methylation reactions 1. Coreaction of [C-12]ethene and [C-13]methanol, J. Catal. 224 (2004) 115–123.
[22] S. Svelle, P.O. Ronning, U. Olsbye, S. Kolboe, Kinetic studies of zeolite-catalyzed methylation reactions. Part 2. Co-reaction of [C-12]propene or [C-12]n-butene and [C-13]methanol, J. Catal. 234 (2005) 385–400.
[23] U. Olsbye, S. Svelle, M. Bjorgen, P. Beato, T.V.W. Janssens, F. Joensen, S. Bordiga, K.P. Lillerud, Conversion of methanol to hydrocarbons: how zeolite cavity and pore size controls product selectivity, Angew. Chemie-Int. Ed. 51 (2012) 5810–5831.
[24] K. Hemelsoet, J. Van der Mynsbrugge, K. De Wispelaere, M. Waroquier, V. Van Speybroeck, Unraveling the Reaction Mechanisms Governing Methanol-to-Olefins Catalysis by Theory and Experiment, ChemPhysChem 14 (2013) 1526–1545.
[25] I. Yarulina, A.D. Chowdhury, F. Meirer, B.M. Weckhuysen, J. Gascon, Recent trends and fundamental insights in the methanol-to-hydrocarbons process, Nat. Catal. 1 (2018) 398–411.
[26] J.F. Haw, D.M. Marcus, Well-defined (supra)molecular structures in zeolite methanol-to-olefin catalysis, Top. Catal. 34 (2005) 41–48.
[27] J.F. Haw, W.G. Song, D.M. Marcus, J.B. Nicholas, The mechanism of methanol to hydrocarbon catalysis, Acc. Chem. Res. 36 (2003) 317–326.
[28] I.M. Dahl, S. Kolboe, On the reaction-mechanism for propene formation in the mto reaction over Sapo-34, Catal. Lett. 20 (1993) 329–336.
[29] I.M. Dahl, S. Kolboe, On the reaction-mechanism for hydrocarbon formation from methanol over Sapo-34.1. Isotopic labeling studies of the co-reaction of ethene and methanol, J. Catal. 149 (1994) 458–464.
[30] I.M. Dahl, S. Kolboe, On the reaction mechanism for hydrocarbon formation from methanol over SAPO-34.2. Isotopic labeling studies of the co-reaction of propene and methanol, J. Catal. 161 (1996) 304–309.
[31] S. Svelle, F. Joensen, J. Nerlov, U. Olsbye, K.P. Lillerud, S. Kolboe, M. Bjorgen, Conversion of methanol into hydrocarbons over zeolite H-ZSM-5: Ethene formation is mechanistically separated from the formation of higher alkenes, J. Am. Chem. Soc. 128 (2006) 14770–14771.
[32] X.Y. Sun, S. Mueller, Y. Liu, H. Shi, G.L. Haller, M. Sanchez-Sanchez, A.C. van Veen, J.A. Lercher, On reaction pathways in the conversion of methanol to hydrocarbons on HZSM-5, J. Catal. 317 (2014) 185–197.
[33] V. Van Speybroeck, K. Hemelsoet, K. De Wispelaere, Q. Qian, J. Van der Mynsbrugge, B. De Sterck, B.M. Weckhuysen, M. Waroquier, Mechanistic studies on chabazite-type methanol-to-olefin catalysts: insights from time-resolved UV/Vis microspectroscopy combined with theoretical simulations, ChemCatChem 5 (2013) 173–184.
[34] K. De Wispelaere, K. Hemelsoet, M. Waroquier, V. Van Speybroeck, Complete low-barrier side-chain route for olefin formation during methanol conversion in H-SAPO-34, J. Catal. 305 (2013) 76–80.
[35] D. Lesthaeghe, B. De Sterck, V. Van Speybroeck, G.B. Marin, M. Waroquier, Zeolite Shape-Selectivity in the gem-Methylation of Aromatic Hydrocarbons, Angew. Chemie – Int. Ed. 46 (2007) 1311–1314.
[36] D.M. McCann, D. Lesthaeghe, P.W. Kletnieks, D.R. Guenther, M.J. Hayman, V. Van Speybroeck, M. Waroquier, J.F. Haw, A complete catalytic cycle for supramolecular methanol-to-olefins conversion by linking theory with experiment, Angew. Chem.-Int. Ed. 47 (2008) 5179–5182.
[37] C.M. Wang, Y.D. Wang, Z.K. Xie, Z.P. Liu, Methanol to olefin conversion on HSAPO-34 zeolite from periodic density functional theory calculations: a complete cycle of side chain hydrocarbon pool mechanism, J. Phys. Chem. C 113 (2009) 4584–4591.
[38] D. Frenkel, B. Smit, Understanding Molecular Simulation, second, edition ed., Academic press, Elsevier, 2002.
[39] K. de Wispelaere, L. Vanduyfhuys, V. Van Speybroeck, Entropy Contributions to Transition State Modeling, in: A. Catlow, V. Van Speybroeck, R.A. Van Santen (Eds.) Modelling and simulation in the science of micro- and Meso-Porous materials Elsevier, 2017, pp. 189-228.
[40] J. Rey, A. Gomez, P. Raybaud, C. Chizallet, T. Bucko, On the origin of the difference between type A and type B skeletal isomerization of alkenes catalyzed by zeolites: the crucial input of ab initio molecular dynamics, J. Catal. 373 (2019) 361–373.
[41] C. Abrams, G. Bussi, Enhanced Sampling in Molecular Dynamics Using Metadynamics Replica-Exchange, and Temperature-Acceleration, Entropy 16 (2014) 163–199.
[42] C.D. Christ, A.E. Mark, W.F. van Gunsteren, Feature article basic ingredients of free energy calculations: a review, J. Comput. Chem. 31 (2010) 1569–1582.
[43] R. Demuynck, S.M.J. Rogge, L. Vanduyfhuys, J. Wieme, M. Waroquier, V. Van Speybroeck, Efficient construction of free energy profiles of breathing metal-organic frameworks using advanced molecular dynamics simulations, J. Chem. Theory Comput. 13 (2017) 5861–5873.
[44] M.A. Cuendet, M.E. Tuckerman, Free energy reconstruction from metadynamics or adiabatic free energy dynamics simulations, J. Chem. Theory Comput. 10 (2014) 2975–2986.
[45] A.C.T. van Duin, S. Dasgupta, F. Lorant, W.A. Goddard, ReaxFF: a reactive force field for hydrocarbons, J. Phys. Chem. A 105 (2001) 9396–9409.
[46] Y. Han, D.D. Jiang, J.L. Zhang, W. Li, Z.X. Gan, J.J. Gu, Development, applications and challenges of ReaxFF reactive force field in molecular simulations, Front. Chem. Sci. Eng. 10 (2016) 16–38.
[47] M. Eichinger, P. Tavan, J. Hutter, M. Parrinello, A hybrid method for solutes in complex solvents: density functional theory combined with empirical force fields, J. Chem. Phys. 110 (1999) 10452–10467.
[48] J. Wieme, K. Lejaeghere, G. Kresse, V. Van Speybroeck, Tuning the balance between dispersion and entropy to design temperature-responsive flexible metal-organic frameworks, Nat. Commun. 9 (2018).
[49] S. Grimme, J. Antony, S. Ehrlich, H. Krieg, A consistent and accurate ab initio parametrization of density functional dispersion correction (DFT-D) for the 94 elements H-Pu, J. Chem. Phys. 132 (2010) 154104.
[50] N. Hansen, T. Kerber, J. Sauer, A.T. Bell, F.J. Keil, Quantum chemical modeling of benzene ethylation over H-ZSM-5 approaching chemical accuracy: a hybrid MP2:DFT study, J. Am. Chem. Soc. 132 (2010) 11525–11538.
[51] B. Peters, Reaction Coordinates and Mechanistic Hypothesis Tests, in: M.A. Johnson, T.J. Martinez (Eds.) Annual Review of Physical Chemistry, Vol 67, 2016, pp. 669-690.
[52] R. Demuynck, J. Wieme, S.M.J. Rogge, K.D. Dedecker, L. Vanduyfhuys, M. Waroquier, V. Van Speybroeck, Protocol for identifying accurate collective variables in enhanced molecular dynamics simulations for the description of structural transformations in flexible metal-organic frameworks, J. Chem. Theory Comput. 14 (2018) 5511–5526.
[53] M.A. Rohrdanz, W.W. Zheng, C. Clementi, Discovering Mountain Passes via Torchlight: Methods for the Definition of Reaction Coordinates and Pathways

in Complex Macromolecular Reactions, in: M.A. Johnson, T.J. Martinez (Eds.) Annual Review of Physical Chemistry, Vol 64, 2013, pp. 295-316.
[54] R.H. Swendsen, J.S. Wang, Replica Monte-Carlo simulation of spin-glasses, Phys. Rev. Lett. 57 (1986) 2607–2609.
[55] Y. Sugita, Y. Okamoto, Replica-exchange molecular dynamics method for protein folding, Chem. Phys. Lett. 314 (1999) 141–151.
[56] Z.F. Jing, L. Xin, H. Sun, Replica exchange reactive molecular dynamics simulations of initial reactions in zeolite synthesis, PCCP 17 (2015) 25421–25428.
[57] G.M. Torrie, J.P. Valleau, Monte-Carlo free-energy estimates using non-boltzmann sampling - application to subcritical lennard-jones fluid, Chem. Phys. Lett. 28 (1974) 578–581.
[58] G.M. Torrie, J.P. Valleau, Non-physical sampling distributions in monte-carlo free-energy estimation - umbrella sampling, J. Comput. Phys. 23 (1977) 187–199.
[59] J. Kastner, Umbrella sampling, Wiley Interdisciplinary Reviews-Computational Molecular, Science 1 (2011) 932–942.
[60] J.G. Kirkwood, Statistical mechanics of fluid mixtures, J. Chem. Phys. 3 (1935) 300–313.
[61] E.A. Carter, G. Ciccotti, J.T. Hynes, R. Kapral, Constrained reaction coordinate dynamics for the simulation of rare events, Chem. Phys. Lett. 156 (1989) 472–477.
[62] T. De Meyer, B. Ensing, S.M.J. Rogge, K. De Clerck, E.J. Meijer, V. Van Speybroeck, Acidity constant (pK(a)) calculation of large solvated dye molecules: evaluation of two advanced molecular dynamics methods, ChemPhysChem 17 (2016) 3447–3459.
[63] W.K. den Otter, W.J. Briels, The calculation of free-energy differences by constrained molecular-dynamics simulations, J. Chem. Phys. 109 (1998) 4139–4146.
[64] E. Paci, G. Ciccotti, M. Ferrario, R. Kapral, Activation-energies by molecular-dynamics with constraints, Chem. Phys. Lett. 176 (1991) 581–587.
[65] T.P. Straatsma, J.A. McCammon, Multiconfiguration thermodynamic integration, J. Chem. Phys. 95 (1991) 1175–1188.
[66] E. Kelly, M. Seth, T. Ziegler, Calculation of free energy profiles for elementary bimolecular reactions by ab initio molecular dynamics: Sampling methods and thermostat considerations, J. Phys. Chem. A 108 (2004) 2167–2180.
[67] M. Iannuzzi, A. Laio, M. Parrinello, Efficient exploration of reactive potential energy surfaces using Car-Parrinello molecular dynamics, Phys. Rev. Lett. 90 (2003) 4.
[68] A. Laio, F.L. Gervasio, Metadynamics: a method to simulate rare events and reconstruct the free energy in biophysics, chemistry and material science, Rep. Prog. Phys. 71 (2008) 126601.
[69] A. Laio, M. Parrinello, Escaping free-energy minima, PNAS 99 (2002) 12562–12566.
[70] I. Bilionis, P.S. Koutsourelakis, Free energy computations by minimization of Kullback-Leibler divergence: An efficient adaptive biasing potential method for sparse representations, J. Comput. Phys. 231 (2012) 3849–3870.
[71] O. Valsson, M. Parrinello, Variational Approach to Enhanced Sampling and Free Energy Calculations, Phys. Rev. Lett. 113 (2014).
[72] O. Valsson, P. Tiwary, M. Parrinello, Enhancing Important Fluctuations: Rare Events and Metadynamics from a Conceptual Viewpoint, in: M.A. Johnson, T.J. Martinez (Eds.) Annual Review of Physical Chemistry, Vol 67, 2016, pp. 159-184.
[73] S. Kumar, J.M. Rosenberg, D. Bouzida, R.H. Swendsen, P.A. Kollman, Multidimensional free-energy calculations using the weighted histogram analysis method, J. Comput. Chem. 16 (1995) 1339–1350.
[74] S. Kumar, D. Bouzida, R.H. Swendsen, P.A. Kollman, J.M. Rosenberg, The weighted histogram analysis method for free-energy calculations on biomolecules.1. The method, J. Comput. Chem. 13 (1992) 1011–1021.
[75] J. Hajek, J. Van der Mynsbrugge, K. De Wispelaere, P. Cnudde, L. Vanduyfhuys, M. Waroquier, V. Van Speybroeck, On the stability and nature of adsorbed pentene in Bronsted acid zeolite H-ZSM-5 at 323 K, J. Catal. 340 (2016) 227–235.
[76] J. Hajek, B. Bueken, M. Waroquier, D. De Vos, V. Van Speybroeck, The Remarkable amphoteric nature of defective UiO-66 in catalytic reactions, ChemCatChem 9 (2017) 2203–2210.
[77] P. Cnudde, K. De Wispelaere, J. Van der Mynsbrugge, M. Waroquier, V. Van Speybroeck, Effect of temperature and branching on the nature and stability of alkene cracking intermediates in H-ZSM-5, J. Catal. 345 (2017) 53–69.
[78] Structure Commission of the International Zeolite Association (IZA-SC), Database of Zeolite structures in, pp. http://www.iza-structure.org/databases/.
[79] J. Dědeček, S. Sklenak, C. Li, B. Wichterlová, V. Gábová, J. Brus, M. Sierka, J. Sauer, Aluminum Siting in the Framework of Silicon Rich Zeolites. A ZSM-5 Study., in: Zeolites and related materials: Trends, targets and challenges, Elsevier, 2008, pp. 781-786.
[80] A. Bhan, Y.V. Joshi, W.N. Delgass, K.T. Thomson, DFT investigation of alkoxide formation from olefins in H-ZSM-5, J. Phys. Chem. B 107 (2003) 10476–10487.
[81] J. Van der Mynsbrugge, K. Hemelsoet, M. Vandichel, M. Waroquier, V. Van Speybroeck, Efficient approach for the computational study of alcohol and nitrile adsorption in H-ZSM-5, J. Phys. Chem. C 116 (2012) 5499–5508.
[82] G. Kresse, J. Furthmuller, Efficient iterative schemes for ab initio total-energy calculations using a plane-wave basis set, Phys. Rev. B 54 (1996) 11169–11186.
[83] G. Kresse, J. Furthmüller, Efficiency of ab-initio total energy calculations for metals and semiconductors using a plane-wave basis set, Comput. Mat. Sci. 6 (1996) 15.
[84] G. Kresse, J. Hafner, *Ab initio* molecular dynamics for liquid metals, Phys. Rev. B 47 (1993) 558–561.
[85] G. Kresse, J. Hafner, Ab initio molecular-dynamics simulation of the liquid-metal-amorphous-semiconductor transition in germanium, Phys. Rev. B 49 (1994) 14251.
[86] Y.K. Zhang, W.T. Yang, Comment on "Generalized gradient approximation made simple", Phys. Rev. Lett. 80 (1998) 890.
[87] K. Yang, J.J. Zheng, Y. Zhao, D.G. Truhlar, Tests of the RPBE, revPBE, tau-HCTHhyb, omega B97X-D, and MOHLYP density functional approximations and 29 others against representative databases for diverse bond energies and barrier heights in catalysis, J. Chem. Phys. 132 (2010) 10.
[88] P.E. Blöchl, Projector augmented-wave method, Phys. Rev. B 50 (1994) 17953.
[89] G. Kresse, D. Joubert, From ultrasoft pseudopotentials to the projector augmented-wave method, Phys. Rev. B 59 (1999) 1758–1775.
[90] A. Heyden, A.T. Bell, F.J. Keil, Efficient methods for finding transition states in chemical reactions: comparison of improved dimer method and partitioned rational function optimization method, J. Chem. Phys. 123 (2005).
[91] P. Pulay, Convergence acceleration of iterative sequences - the case of scf iteration, Chem. Phys. Lett. 73 (1980) 393–398.
[92] W.H. Press, B.P. Flannery, S.A. Teukolsky, W.T. Vetterling, Numerical Recipes: The Art of Scientific Computing, Cambridge Univ. Press, New York, 1986.
[93] B.A. De Moor, A. Ghysels, M.-F. Reyniers, V. Van Speybroeck, M. Waroquier, G. B. Marin, Normal mode analysis in zeolites: toward an efficient calculation of adsorption entropies, J. Chem. Theory Comput. 7 (2011) 1090–1101.
[94] A. Ghysels, T. Verstraelen, K. Hemelsoet, M. Waroquier, V. Van Speybroeck, TAMkin: A versatile package for vibrational analysis and chemical kinetics, J. Chem. Inf. Model. 50 (2010) 1736–1750.
[95] J. Hutter, M. Iannuzzi, F. Schiffmann, J. VandeVondele, CP2K: atomistic simulations of condensed matter systems, wiley interdisciplinary reviews-computational molecular, Science 4 (2014) 15–25.
[96] J. VandeVondele, M. Krack, F. Mohamed, M. Parrinello, T. Chassaing, J. Hutter, QUICKSTEP: Fast and accurate density functional calculations using a mixed Gaussian and plane waves approach, Comput. Phys. Commun. 167 (2005) 103–128.
[97] G.J. Martyna, D.J. Tobias, M.L. Klein, Constant-pressure molecular-dynamics algorithms, J. Chem. Phys. 101 (1994) 4177–4189.
[98] G. Lippert, J. Hutter, M. Parrinello, A hybrid Gaussian and plane wave density functional scheme, Mol. Phys. 92 (1997) 477–487.
[99] G. Lippert, J. Hutter, M. Parrinello, The Gaussian and augmented-plane-wave density functional method for ab initio molecular dynamics simulations, Theor. Chem. Acc. 103 (1999) 124–140.
[100] S. Goedecker, M. Teter, J. Hutter, Separable dual-space Gaussian pseudopotentials, Physical Review B 54 (1996) 1703–1710.
[101] J. Van der Mynsbrugge, S.L.C. Moors, K. De Wispelaere, V. Van Speybroeck, Insight into the Formation and Reactivity of Framework-Bound Methoxide Species in H-ZSM-5 from Static and Dynamic Molecular Simulations, ChemCatChem 6 (2014) 1906–1918.
[102] S.L.C. Moors, K. De Wispelaere, J. Van der Mynsbrugge, M. Waroquier, V. Van Speybroeck, Molecular Dynamics Kinetic Study on the Zeolite-Catalyzed Benzene Methylation in ZSM-5, ACS Catal. 3 (2013) 2556–2567.
[103] B. Ensing, A. Laio, M. Parrinello, M.L. Klein, A recipe for the computation of the free energy barrier and the lowest free energy path of concerted reactions, J. Phys. Chem. B 109 (2005) 6676–6687.
[104] M. Bonomi, D. Branduardi, G. Bussi, C. Camilloni, D. Provasi, P. Raiteri, D. Donadio, F. Marinelli, F. Pietrucci, R.A. Broglia, M. Parrinello, PLUMED: A portable plugin for free-energy calculations with molecular dynamics, Comput. Phys. Commun. 180 (2009) 1961–1972.
[105] M. Souaille, B. Roux, Extension to the weighted histogram analysis method: combining umbrella sampling with free energy calculations, Comput. Phys. Commun. 135 (2001) 40–57.
[106] J. Kastner, W. Thiel, Bridging the gap between thermodynamic integration and umbrella sampling provides a novel analysis method: "umbrella integration", J. Chem. Phys. 123 (2005).
[107] M. Kilic, B. Ensing, Acidity constants of lumiflavin from first principles molecular dynamics simulations, PCCP 16 (2014) 18993–19000.
[108] S. Bailleul, S.M.J. Rogge, L. Vanduyfhuys, V. Van Speybroeck, Insight into the Role of Water on the Methylation of Hexamethylbenzene in H-SAPO-34 from First Principle Molecular Dynamics Simulations, ChemCatChem 11 (2019) 3993–4010.
[109] P. Cnudde, K. De Wispelaere, L. Vanduyfhuys, R. Demuynck, J. Van der Mynsbrugge, M. Waroquier, V. Van Speybroeck, How Chain Length and Branching Influence the Alkene Cracking Reactivity on H-ZSM-5, ACS Catal. 8 (2018) 9579–9595.
[110] P.W. Atkins, Physical Chemistry, Oxford.
[111] T. Bucko, S. Chibani, J.F. Paul, L. Cantrel, M. Badawi, Dissociative iodomethane adsorption on Ag-MOR and the formation of AgI clusters: an & ITab initio&IT molecular dynamics study, PCCP 19 (2017) 27530–27543.
[112] B. De Sterck, R. Vaneerdeweg, F. Du Prez, M. Waroquier, V. Van Speybroeck, Solvent Effects on Free Radical Polymerization Reactions: The Influence of Water on the Propagation Rate of Acrylamide and Methacrylamide, Macromolecules 43 (2010) 827–836.
[113] S. Jakobtorweihen, N. Hansen, F.J. Keil, Molecular simulation of alkene adsorption in zeolites, Mol. Phys. 103 (2005) 471–489.

[114] S.N. Steinmann, C. Corminboeuf, Comprehensive bench marking of a density-dependent dispersion correction, J. Chem. Theory Comput. 7 (2011) 3567–3577.
[115] S.N. Steinmann, C. Corminboeuf, A generalized-gradient approximation exchange hole model for dispersion coefficients, J. Chem. Phys. 134 (2011).
[116] M. Dion, H. Rydberg, E. Schroder, D.C. Langreth, B.I. Lundqvist, Van der Waals density functional for general geometries, Phys. Rev. Lett. 92 (2004) 246401.
[117] J. Klimes, D.R. Bowler, A. Michaelides, Van der Waals density functionals applied to solids, Physical Review B 83 (2011).
[118] D.G. Truhlar, B.C. Garrett, S.J. Klippenstein, Current status of transition-state theory, J. Phys. Chem. 100 (1996) 12771–12800.
[119] H. Eyring, The activated complex in chemical reactions, J. Chem. Phys. 3 (1935) 107–115.
[120] W.F.K. Wynne-Jones, H. Eyring, The Absolute Rate of Reactions in Condensed Phases, J. Chem. Phys. 3 (1935) 492–502.
[121] M.G. Evans, M. Polanyi, Somer Applications of the Transition State Method to the Calculation of Reaction Velocities, especially in Solution, Trans. Faraday Soc. 31 (1935) 875–894.
[122] G. Ciccotti, M. Ferrario, Blue moon approach to rare events, Mol. Simul. 30 (2004) 787–793.
[123] P. Hanggi, P. Talkner, M. Borkovec, Reaction-rate theory - 50 years after kramers, Rev. Mod. Phys. 62 (1990) 251–341.
[124] B.J. Berne, M. Borkovec, J.E. Straub, Classical and modern methods in reaction-rate theory, J. Phys. Chem. 92 (1988) 3711–3725.